Design of Air and Liquid Cooling Systems for Electronic Components Using Concurrent Simulation and Experiment

Tunc Icoz
Thermal Scientist
GE Global Research,
One Research Circle,
Niskayuna NY 12309

Nitin Verma
Graduate Assistant
Rutgers University,
Dept. Mechanical & Aerospace Eng.,
New Brunswick, NJ 08901, USA

Yogesh Jaluria[1]
Board of Governors Professor
Fellow, ASME
Rutgers University,
Dept. Mechanical & Aerospace Eng.,
New Brunswick, NJ 08901

The design of cooling systems for electronic equipment is getting more involved and challenging due to increase in demand for faster and more reliable electronic systems. Therefore, robust and more efficient design and optimization methodologies are required. Conventional approaches are based on sequential use of numerical simulation and experiment. Thus, they fail to use certain advantages of using both tools concurrently. The present study is aimed at combining simulation and experiment in a concurrent manner such that outputs of each approach drive the other to achieve better engineering design in a more efficient way. In this study, a relatively simple problem, involving heat transfer from multiple heat sources simulating electronic components and located in a horizontal channel, was investigated. Two experimental setups were fabricated for air and liquid cooling experiments to study the effects of different coolants. De-ionized water was used as the liquid coolant in one case and air in the other. The effects of separation distance and flow conditions on the heat transfer and on the fluid flow characteristics were investigated in detail for both coolants. Cooling capabilities of different cooling arrangements were compared and the results from simulations and experiments were combined to create response surfaces and to find the optimal values of the design parameters.
[DOI: 10.1115/1.2353284]

Keywords: air cooling of electronic systems, liquid cooling, concurrent simulation and experiment, design optimization, channel flow

Introduction

The performance of an electronic system is strongly related to its thermal management. Increase in power density and data processing speed as results of advances in micro- and nano-scale manufacturing and packaging technologies bring new challenges to the thermal management problem. A significant fraction of device failures is attributed to poor thermal control and, moreover, the decrease in heat transfer areas, demands for more reliable systems, and economical considerations make an acceptable or optimal design even more difficult.

Air continues to be the most widely used coolant in electronic systems due to its availability, low operational cost, and easy maintenance. Mixed convection heat transfer is a very common air cooling arrangement, where the air flow is provided by means of a fan or a blower. A literature review on heat transfer in electronic equipment cooling was presented in [1,2]. The papers on mixed air convection, published in 2000, were reviewed in [3]. Kang and Jaluria [4] studied the mixed convection heat transfer from a single protruding heat source mounted on a vertical wall in an external flow. Tewari and Jaluria [5] presented an experimental study on mixed convection from multiple heat sources mounted on horizontal and vertical surfaces and investigated the effect of separation distance on heat transfer from the components. Papanicolaou and Jaluria [6] numerically investigated mixed convection heat transfer from a single flush mounted heat source located in an enclosure for different Re in the range of 50–2000 and for the mixed convection parameter Gr/Re^2 in the range of 0–10. Nakayama and Park [7] carried out an experimental and numerical work on conjugate heat transfer from a single heat source in a channel for air velocities between 1 and 7 m/s. They used experimentation to investigate the heat transfer characteristics and to supply boundary condition information for the numerical study of conduction in the surface. Mixed convection from multiple layered boards with periodic boundary conditions was studied numerically by Kim et al. [8] for Re in the range of 100–1500 and Gr in the range of $0-2\times10^6$. Rahman and Raghavan [9] numerically studied the transient response of protruding modules in horizontal cross flow.

Oscillatory flow is a common phenomena encountered in electronic cooling applications. It has been found that inducing oscillations in the driving flow enhances the heat transfer rates from the heat sources [10–12]. Stability and self-sustained oscillations have been studied in detail in [13–15].

Although air cooling continues to be the most widely used method for cooling electronic packages, it has long been recognized that significantly higher heat fluxes can be accommodated through the use of liquid cooling. Sathe and Joshi [16] investigated natural convection arising from a heat generating substrate-mounted protrusion in a liquid-filled two-dimensional enclosure. Gupta and Jaluria [17] performed experiments to study forced convection heat transfer from an array of protruding heat sources mounted in a rectangular duct using de-ionized water. Park and Bergles [18] studied the natural convection heat transfer from simulated heat sources of varying height and width in water and R-113. Joshi et al. [19] investigated the immersion cooling of an array of rectangular protrusions in different dielectric liquids and came up with the result that heat transfer increases with the increase in enclosure height, though this dependence was weak.

[1]Corresponding author; jaluria@jove.rutgers.edu
Contributed by the Electronic and Photonic Packaging Division of ASME for publication in the JOURNAL OF ELECTRONIC PACKAGING. Manuscript received January 9, 2006; final manuscript received March 27, 2006. Review conducted by Giulio Lorenzini. Paper presented at the 2004 ASME Heat Transfer/Fluids Engineering Summer Conference (HT-FED2004), July 11, 2004 - July 15, 2004, Charlotte, North Carolina, USA.

 Copyright © 2006 by ASME

Downloaded From: http://electronicpackaging.asmedigitalcollection.asme.org/ on 08/21/2016 Terms of Use: http://www.asme.org/about-asme/terms-of-use

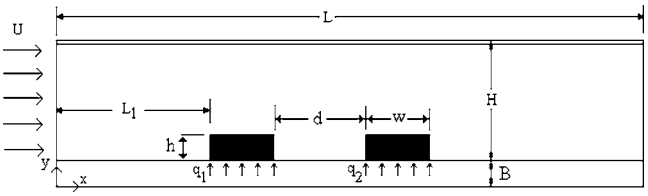


Fig. 1 Two heating elements in a channel, simulating electronic components

Incropera et al. [20] carried out an experimental study on convection heat transfer from flush mounted heat sources using water and FC77. They observed that there is a significant reduction in the heat transfer rate from the first to the second row. For the rest of the rows downstream this reduction was found to be 5%.

The conventional engineering design and optimization are based on sequential use of computer simulation and experiment [21]. However, the conventional methods fail to use the advantages of using experiment and simulation concurrently in real time. The objective of the present study is to use concurrent simulation and experiment for design of cooling systems for electronic equipment, which consists of multiple heat sources in a channel. The details of this methodology are presented in [22–24]. The effects of different coolants, air and de-ionized water, separation distances of heat sources and flow conditions on heat removal rate, and on pressure change are investigated. The results are used as inputs for system design and optimization, employing different criteria or objective functions.

Problem Description

The simple physical system considered here, as shown in Fig. 1, consists of single and multiple identical heat sources, which approximate electronic components, located in a horizontal channel, which is wide in the transverse direction and thus yields a two-dimensional configuration. The one on the left is designated as the first heat source. Their height and width are h and w, respectively. Heat sources are separated by distance d. The thickness of the bottom plate is B.

The problem is removing the energy dissipated by these components by the flow of air or de-ionized water. The focus here is on air cooling and water-cooling results are used to indicate similar trends. The flow conditions are defined by Re and Gr, both being based on the channel height. The fluid is represented by its properties particularly the Prandtl number Pr. Design variables include the inlet fluid velocity, heat input to the components, channel dimensions, coolant, location, and orientation of the heat sources. Typical design objectives are maximizing the heat removal rate from the components and minimizing the pressure drop. As constraints, the temperature and pressure drop have to be kept below some allowable limits, i.e., T_{wo}, ΔP_o.

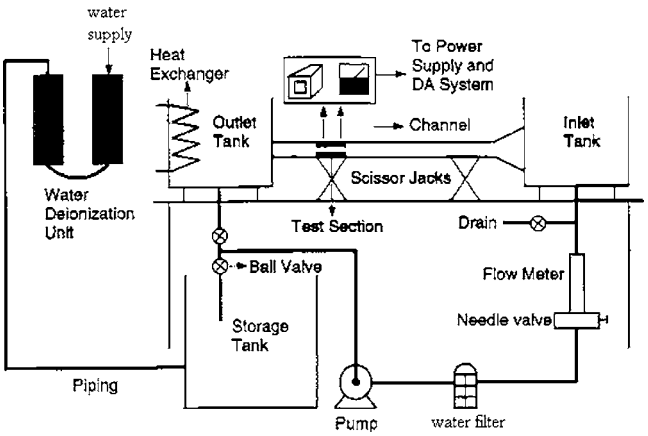


Fig. 3 Experimental system for liquid cooling section for air cooling

Numerical and experimental methods are to be used to study a wide range of design variables and operating conditions. The overall inputs required for the design and optimization of the system are obtained using numerical simulation for low flow rates and heat inputs and experimental systems for larger values. The switch from simulation to experiment is determined based on the critical values of Re and Gr values for transition to turbulence.

Experimental Systems

Two experimental setups have been used in this study, one for air and the other for liquid cooling. The system for air-cooling experiments is shown in Fig. 2. A rectangular cross section horizontal channel, having a height of $H=54$ mm and a width of $W=320$ mm, is made from Plexiglas. A converging inlet section, a stagnation chamber, and a honeycomb filter are used to assure the uniformity of incoming flow. The airflow rate is controlled by a data acquisition system by means of a proportional flow control valve. Three K-type thermocouples and two heat flux sensors are installed in each heat source to monitor the temperatures and heat dissipation rates. The air velocity is measured using a pitot tube. The pressure drop across the test section is measured using static pressure probes connected to a pressure transducer. Kapton flexible heaters are used to provide the heat input to the sources. The width, w, of the protruding elements is set at $0.5H$, i.e., $w=25.4$ mm. The separation distance, d, between two heat sources is set at $2w$. The experiments for air are performed for Re $=1800-5200$.

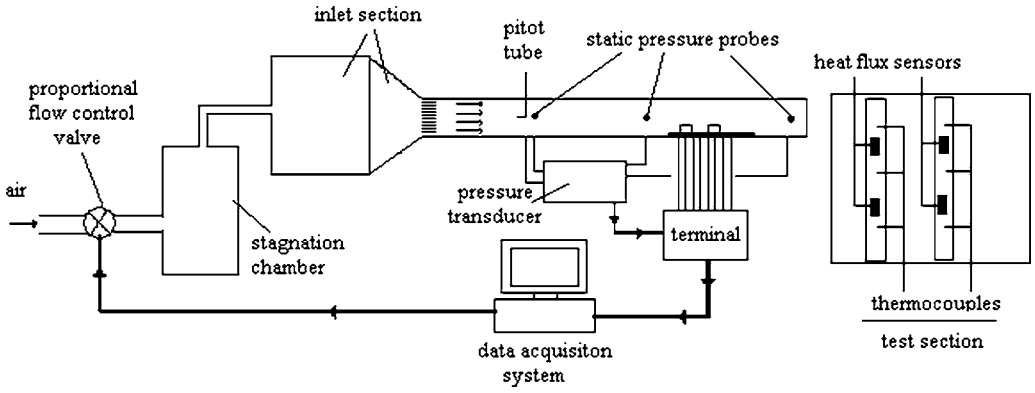


Fig. 2 Experimental system and test

Downloaded From: http://electronicpackaging.asmedigitalcollection.asme.org/ on 08/21/2016 Terms of Use: http://www.asme.org/about-asme/terms-of-use

Figure 3 displays the schematic diagram of the experimental apparatus used for liquid-cooling experiments. Two identical flush mounted heat sources are attached to the bottom surface of a rectangular channel. Two thermocouples are installed on each heating element to measure the surface temperature. The flow of the liquid is provided by means of a pump and a flow meter is used to measure the volumetric flow rate. De-ionized water is used as the liquid coolant to investigate the forced convective heat transfer from multiple flush mounted heat sources. The concurrent numerical-experimental approach is largely demonstrated for air cooling, with water cooling considered for comparison and as another variable for design and optimization.

The liquid cooling experiments are performed to study the free and mixed convective heat transfer characteristics of two flush mounted discrete heat sources. The Reynolds number based on the channel height is varied in the range from 2800 to 5800. Natural convection for the same geometrical configuration has also been investigated. Local temperature measurements are made by six thermocouples along the uniformly heated surface parallel to the flow direction. Stream-wise spacing, d, is varied from half to four times the width of heat source (i.e., $d=0.5-4w$). Natural air-cooling experiments are also performed to compare the cooling capabilities of different coolants.

In order to get the maximum heat transfer rates from the heat sources, the surface temperatures are set at 60°C for all experiments presented later in this study. The steady state is assumed when the temperatures of the heat sources do not change more than ±0.3° around 60°C for 15 min. The total uncertainty of the heat transfer rate measurement is found to be ±4.2 W/m. The uncertainty in the pressure drop is ±0.13 Pa, and the Reynolds number is estimated within ±250 in the experiments.

Numerical Simulation

Numerical simulation can be used very satisfactorily for low Re and Gr values. The governing non-dimensional differential equations for laminar mixed convection flow, with constant thermophysical properties, can be written in the following form: Mass, momentum and energy equations within the flow field (i.e., $X > B/H$):

$$\nabla \cdot V = 0 \tag{1}$$

$$\frac{\partial V}{\partial \tau} + V \cdot \nabla V = -\nabla P + \frac{1}{\mathrm{Re}} \nabla^2 V - \frac{\mathrm{Gr}}{\mathrm{Re}^2} \theta \cdot g \tag{2}$$

$$\frac{\partial \theta}{\partial \tau} + V \cdot \nabla \theta = \frac{1}{\mathrm{RePr}} \nabla^2 \theta \tag{3}$$

Conduction equation within the bottom plate (substrate):

$$\frac{\partial \theta}{\partial \tau} = \frac{1}{\mathrm{RePr}} \nabla^2 \theta \tag{4}$$

where the dimensionless variables are defined as:

$$X = \frac{x}{H}; \quad Y = \frac{y}{H}; \quad U = \frac{u}{U_m}; \quad V = \frac{v}{U_m} \tag{5}$$

$$\tau = t \frac{U_m}{H}; \quad \theta = \frac{T - T_0}{T_s - T_0}; \; P = \frac{p - p_0}{\rho U_m^2} \tag{6}$$

$$\mathrm{Gr} = \frac{g\beta \cdot h^3 (T_s - T_0)}{v^2}; \quad \mathrm{Pr} = \frac{v}{\alpha}; \; \beta = -\frac{1}{\rho}\left(\frac{\rho - \rho_0}{T - T_0}\right) \tag{7}$$

The boundary conditions implemented here can be summarized as follows.

Uniform axial and zero vertical velocity at the inlet at ambient temperature

Table 1 Grid dependence study

	Re=600		Re=1200	
Grid size	Nu_1	Nu_2	Nu_1	Nu_2
151×48	9.742	9.476	11.547	14.261
251×68	10.635	9.423	12.758	13.308
351×88	10.641	9.418	12.824	13.105

$$U = 1; \quad V = 0; \quad \theta = 0; \quad \text{at } X = 0 \tag{8}$$

Fully developed flow conditions at the exit;

$$\frac{\partial U}{\partial X} = 0; \quad V = 0; \quad \frac{\partial \theta}{\partial X} = 0; \quad \text{at } X = L/H \tag{9}$$

No-slip conditions and adiabatic surface assumption at top and bottom walls;

$$U = 0; \quad V = 0; \quad \frac{\partial \theta}{\partial X} = 0; \quad \text{at } Y = 0 \text{ and } (B+H)/H \tag{10}$$

The local convective heat transfer from the heat sources is described by the local Nusselt number, Nu, defined as:

$$\mathrm{Nu} = \frac{h_c \,.\, h}{k} = \left(\frac{\partial \theta}{\partial n}\right)_{C_{hs}} \tag{11}$$

The average convective heat transfer coefficient, h_{av} is defined as:

$$h_{av} = \int_{C_{hs}} h_c(n) dn \tag{12}$$

and the average Nusselt number, Nu_{av} is:

$$\mathrm{Nu}_{av} = \frac{h_{av} h}{k} \tag{13}$$

The preceding governing equations are solved using the finite volume method for primitive variables on a non-uniform staggered grid. Pressure calculations are done using a scheme similar to the SIMPLER algorithm, as explained in [25] in detail. The alternating direction implicit method is used to solve the governing differential equations. Further details on the numerical scheme and analysis can be obtained from [12,26].

A grid independence test is performed to find the appropriate grid size. Nusselt numbers of both of the heat sources are given for different grid sizes in Table 1. The results obtained with a 251×68 grid ensured good a compromise between accuracy and computational time and has been used for the rest of the computations. The convergence criteria and the numerical parameters were also varied to make sure that their effect on the results was negligible.

To validate the code the computed results are compared to the results obtained by Kim et al. [12] for a forced air convection in a channel problem when Re=750. The local Nusselt number along the first heat source surface is plotted, as shown in Fig. 4, and two results showed good agreement, validating the present results.

Results and Discussion. The temperature and velocity distributions, the heat removal rates, and pressure drop are calculated using the described simulation code for laminar flows, as well as the beginning of oscillatory flow. Experiments are used for translational and turbulent flows.

The first part of the simulation results deals with the determination of the critical flow conditions up to which numerical simulation can be used satisfactorily. The Gr value, which is set at 7.2×10^5, is constant for all computations because the heat sources are treated as isothermal elements, at a temperature of 60°C above ambient, and the channel height, which is kept constant throughout the study, is chosen as the characteristic length

Downloaded From: http://electronicpackaging.asmedigitalcollection.asme.org/ on 08/21/2016 Terms of Use: http://www.asme.org/about-asme/terms-of-use

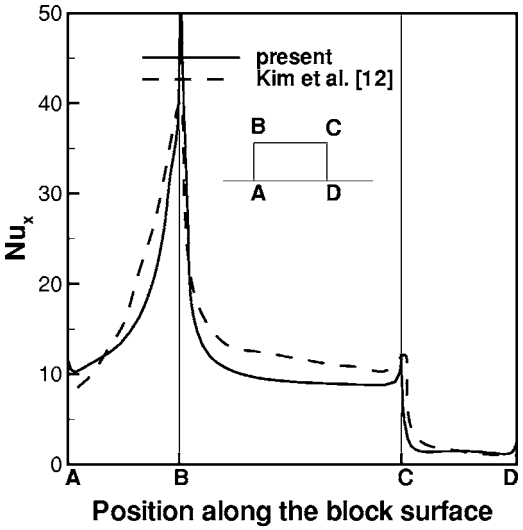


Fig. 4 Comparison of computed local Nu at the first source for forced convection at Re=750 without a vortex promoter

for non-dimensional parameters, such as Re and Gr. The critical Re value is determined by observing the transient change in Nu values as a function of time for different Re values. Figure 5 displays the transient response of Nu for two different heat source heights, i.e., $h=0.25H$ and $h=0.35H$, when the heat sources are separated with a distance of $d=2w$. The transient results reveal that the onset of unsteady flow starts at around Re=1500.

The numerical and experimental results are combined for the design optimization of the air-cooling system described earlier. First, the agreement between the results obtained using the two methods is studied. Figure 6 displays both the computed and experimental results. A discontinuity, in the first heat source heat transfer rate, is observed when the switch from simulation to experiment occurs. This is attributed to the turbulence at the incoming airflow and three-dimensional effects. The incoming velocity profiles across the flow cross section showed slight irregularities at the inflow, as depicted in Fig. 7, even though various cautionary measures are applied, such as placing screens, filters and a converging inlet. In real life applications, the turbulence at the inlet always exists to some extent, whereas the numerical simulation assumes no initial turbulence at all thus, causing this discrepancy. This has, of course, been seen in other flows as well, such as flows in tubes and pipes. For the second heat source heat transfer rate, however, very good agreement is found between the numerical

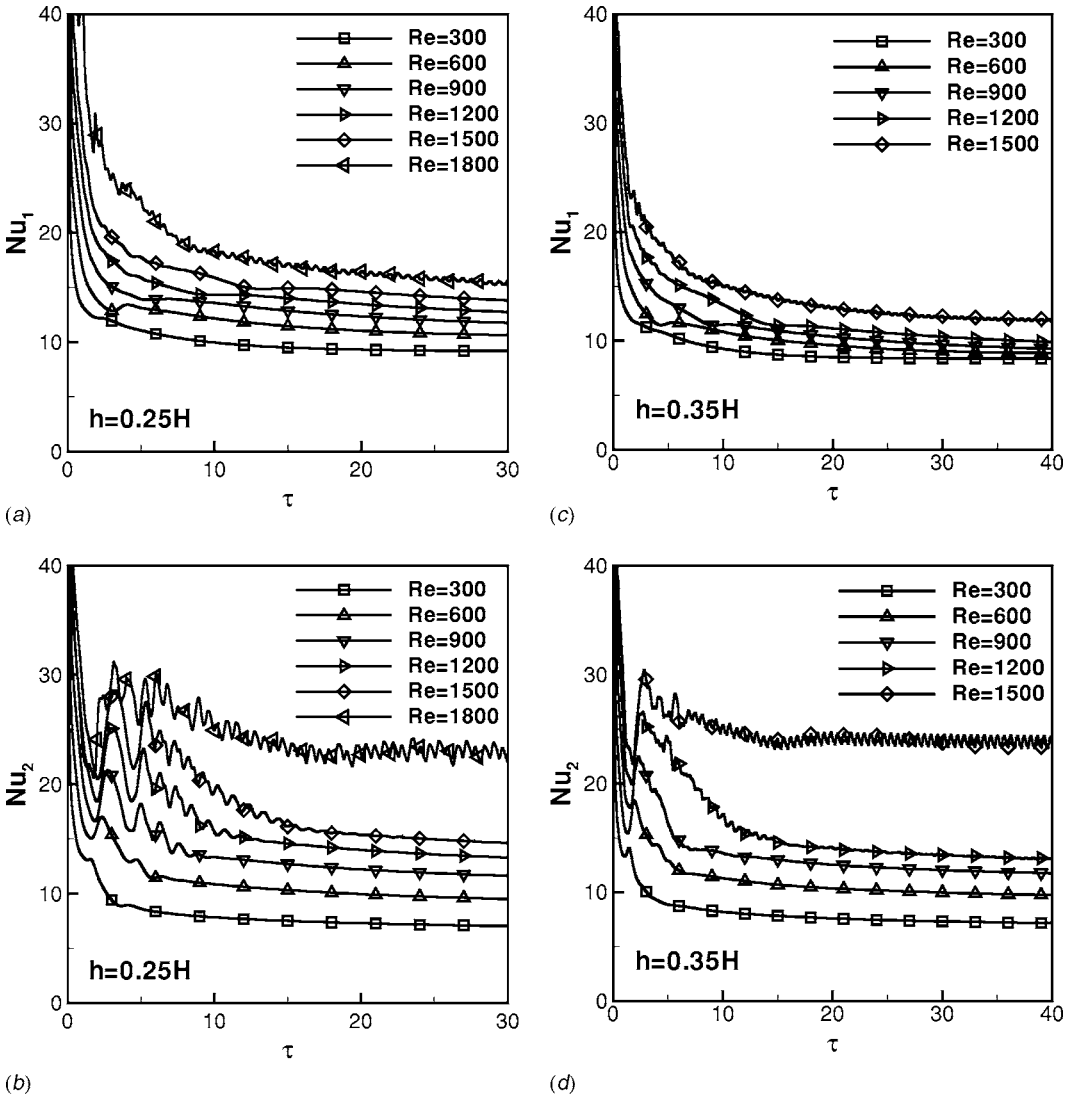
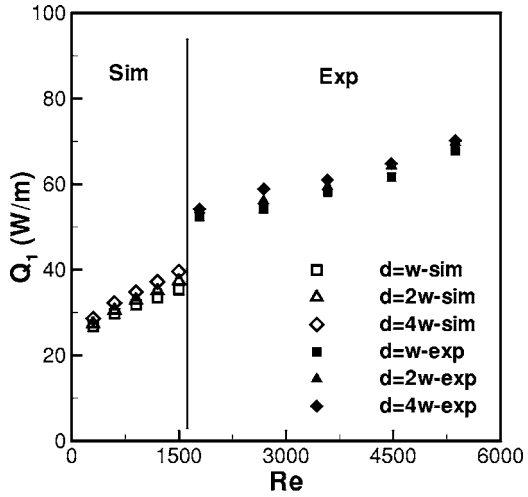
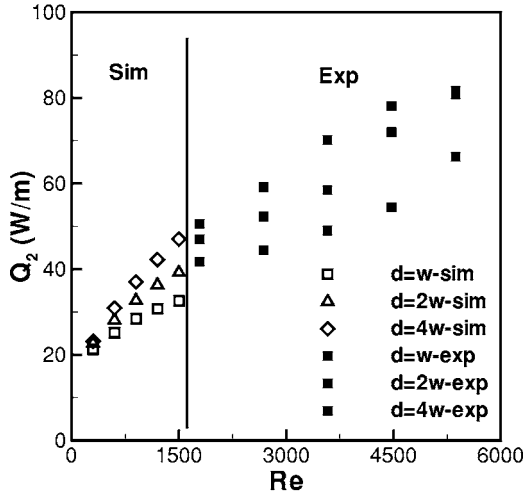


Fig. 5 Transient variations of Nu_1 and Nu_2 for $d=2w$ (*a*,*b*) $h=0.25H$, and (*c*,*d*) $h=0.35H$

Downloaded From: http://electronicpackaging.asmedigitalcollection.asme.org/ on 08/21/2016 Terms of Use: http://www.asme.org/about-asme/terms-of-use



(*a*)



(*b*)

Fig. 6 Computed and measured heat transfer rates as functions of Re and *d* when *h*/*H*=0.25 from (*a*) first heat source, and (*b*) second heat source

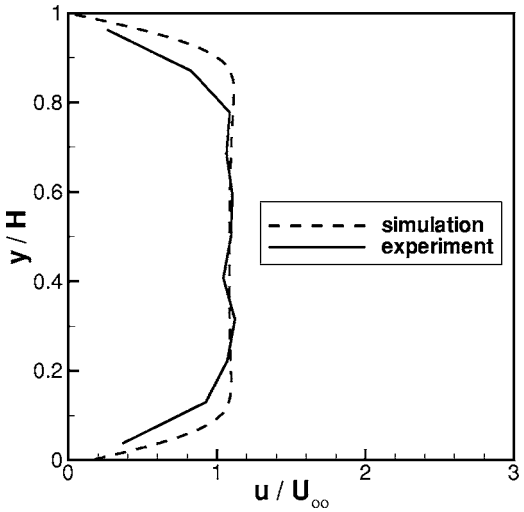


Fig. 7 Comparison of experimental velocity profile with the profile obtained using numerical simulation for U_∞=0.45 m/s, Re=1500

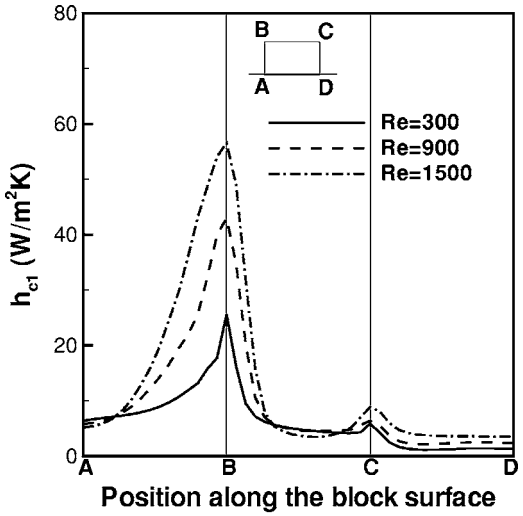
and experimental results, since the wakes created by the first source are very well modeled numerically, leading to experimentally comparable computational results.

The heat transfer rates and pressure drop are computed when $h/H=0.25$. Re is varied from 300 to 1500 and measured experimentally for Re from 1500 to 5600, when d varied between w and $4w$. Figure 6 shows the heat transfer rate results obtained using numerical simulation and experiments for both of the heating elements. The enhanced mixing of cold air with the heated air with Re, and as a result, reduced air temperatures between the two heat sources causes an increase in the heat transfer rates from both components. The effect of Re and d are more significant for the heat source downstream, due to circulation zones being closer to the second heat source. This is attributed to the enhanced heat removal rates along the entire heat transfer surface of second heat source, as depicted in Fig. 8. The major increase in the first heat source heat transfer rate takes place on the upstream face and at a very small area in the vicinity of the top left corner. However, along the top and downstream surfaces, Re has almost no affect on local convective heat transfer coefficient, (h_c=Nu.k/H) of the first heat source. As a result, the increase in heat transfer rate from the first heat source is limited to 30–40%, whereas it reaches 50–80% for the second heat source in the laminar flow region. In this flow regime, the separation distance is found to enhance heat transfer rate from the first heat source about 7–12%, which is not very significant in the laminar region. This is attributed to the fact that the enhancement is only along the surface facing to the second heat source, as depicted in Fig. 9. Except for this surface, the separation distance has no effect on the heat removal from the first heat source. However, greater separation distances reduce the air temperature between the heat sources by letting more cold air into this region. The result for the second heat source reveals this phenomenon much more clearly. The increase in the convective heat transfer coefficient at the second heat source is observed to take place at the left surface. The enhancement in the heat transfer rate from the second heat source is found to be 9–44% as separation distance increases from w to $4w$. In the turbulent region, experimental results reveal that the effect of d is much more significant on the second heat source than the first source. The enhancement in the heat transfer rate is just about 3–5% for the first heat source, whereas up to 60% increase in heat removal rate is achieved from the second heat source by changing d from w to $4w$ at Re=3300. Because the flow becomes turbulent a much better mixing, which takes place between the heat sources, can be obtained as the heat sources are placed farther apart from each other. This in turn reduces local air temperatures and increases the heat transfer rate from the heat source located downstream.

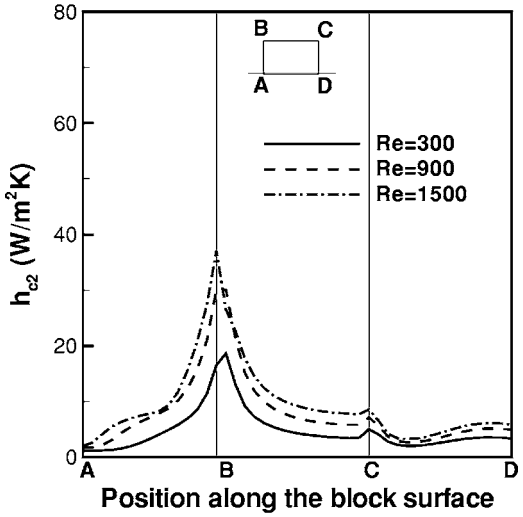
The pressure drop results are also found to be in good agreement, as shown in Fig. 10. The experimental values are found to be about 15% less than is projected by the computational results at around Re=1500. The computational results show that a severe increase in ΔP, about 400%, occurs as Re is raised from 300 to 1500. The effect of separation distance on the same parameter, however, is found to be small in the same Re range, increasing ΔP less than 8%. This negligible effect of separation distance on pressure loss, however, becomes severe in the turbulent flow regime. The stronger vortices and enhanced mixing are the two major contributors to the pressure drop, resulting in an increase of more than 50% as d is changed from w to $4w$ at Re=4500.

The last design variable is chosen to be the heat source height. It is desired to have minimal protrusion because of two reasons. Not only, for it cause additional cost to the design as more material is consumed as heat sink, but also, it increases the pressure requirement. The advantage of having higher surfaces is that it enhances the heat removal from the components by simply increasing the heat transfer area. Figure 11 shows the streamlines of the flow for Re=900 when d is set at $2w$. The streamlines reveal

Downloaded From: http://electronicpackaging.asmedigitalcollection.asme.org/ on 08/21/2016 Terms of Use: http://www.asme.org/about-asme/terms-of-use

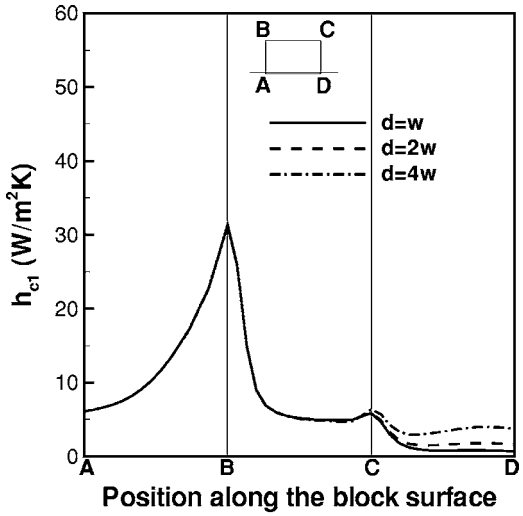


(*a*)

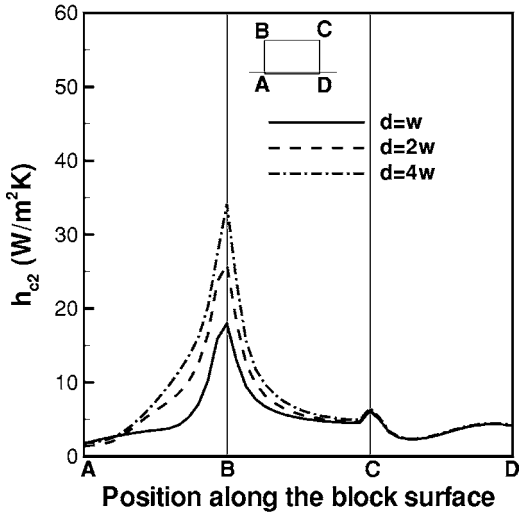


(*b*)

Fig. 8 Local h_c when $h/H=0.25$ and $d=2w$ of (*a*) first heat source and (*b*) second heat source



(*a*)



(*b*)

Fig. 9 Local h_c when $h/H=0.25$ and Re=600 (*a*) first heat source and (*b*) second heat source

that higher protrusions cause more vigorous secondary flows. Especially, the circulation zone between the heat sources is much closer to the source in the downstream, causing better mixing and enhancing heat removal from the second heat source.

As the air is forced through a smaller cross section, the velocity increases above the heat sources, as shown in Fig. 12(*a*), resulting in higher convective heat transfer coefficients. However, due to higher sidewalls, which cold air passes by before reaching the top surface, the temperature of the air increases as it passes the sidewalls, as depicted in Fig. 12(*b*). This results in thicker boundary layers along the top surface of the heat sources, which reduces the heat removal rate from the thermal sources. Figure 13 displays the local h_c along the top surface of the heat sources for different heights. It is found in the laminar flow regime that the convective heat transfer coefficient decreases significantly along the top surface of the first heat source as the source height increases. This observation leads to the conclusion that the increase in air temperature and consequently in the boundary layer thickness dominates the enhancing effect of greater air velocities. However, the effect of increased heat transfer surface is found to be most dominant since there is a net enhancement of about 15–30% observed in the heat removal rate, as displayed in Fig. 13. For the second

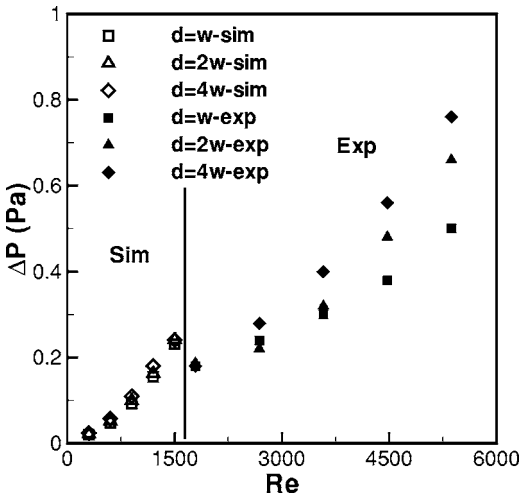


Fig. 10 Computational and experimental results of ΔP

Downloaded From: http://electronicpackaging.asmedigitalcollection.asme.org/ on 08/21/2016 Terms of Use: http://www.asme.org/about-asme/terms-of-use

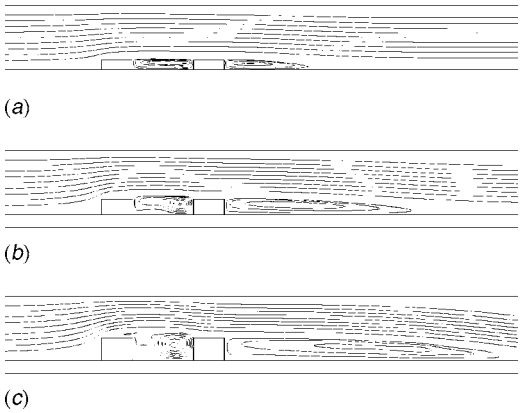


Fig. 11 Streamlines at Re=900 and $d=2w$ when (*a*) $h/H=0.15$, (*b*) $h/H=0.25$, and (c) $h/H=0.35$

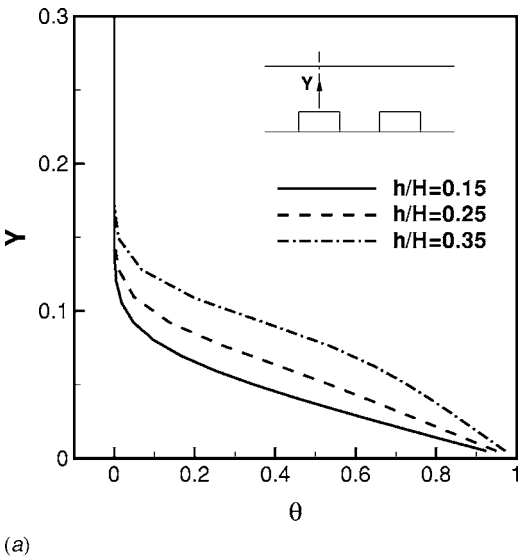


Fig. 12 Computed (*a*) temperature profiles, (*b*) axial velocity profiles, above the first heat source at Re=900 and $d=2w$ for different heat source heights

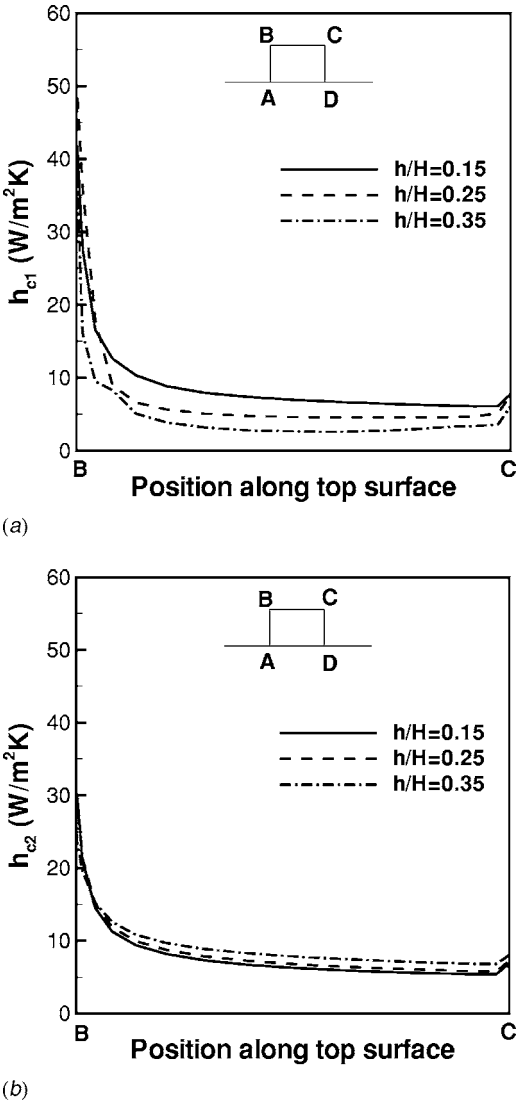
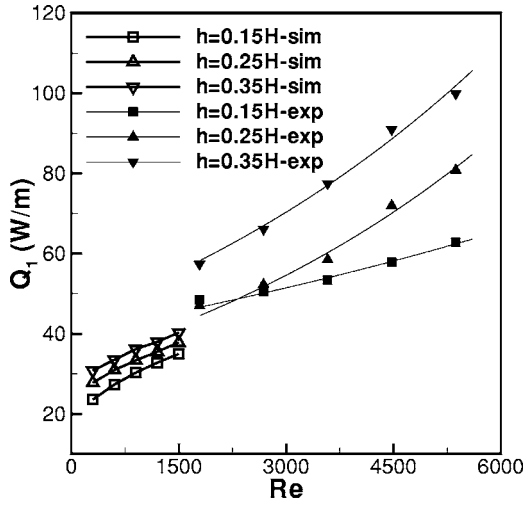


Fig. 13 Local h_c at Re=900 and $d=2w$ along the top wall (*a*) h_{c1} and (*b*) h_{c2}

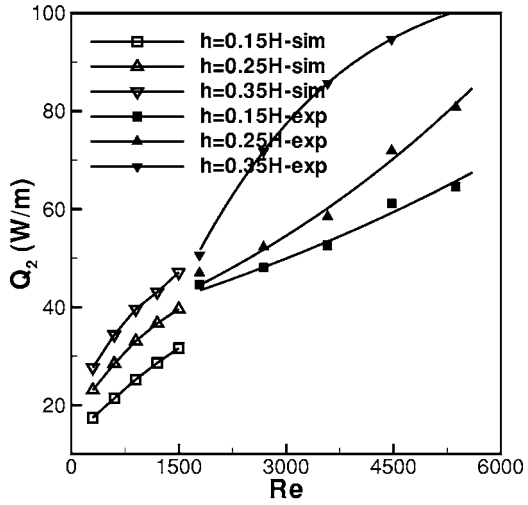
heat source, on the other hand, in addition to the increase in heat transfer surface, the heat transfer coefficient also increases. This combined effect leads to much larger enhancement in heat transfer rate, about 60–125%, from the second heat source. The results indicate that the enhancement in the heat transfer rates is greatest when the heat source height is increased. The turbulent flow results, as shown in Fig. 14, show that almost twice the heat transfer rate can be achieved from the first heat source by increasing h/H from 0.15 to 0.35. The difference between two heat sources is observed to be small. However, the pressure drop is found to increase drastically with h/H, as shown in Fig. 15. About 200% increase in ΔP is observed when h/H ratio is increased from 0.15 to 0.35 for the laminar flow. The effect of the heat source height on the pressure drop for the turbulent flows is found to be profound, especially when h/H is changed from 0.25 to 0.35, as displayed in Fig. 5.24. This increase in protrusion height causes almost 200% raise in the pressure drop. At Re=5600 the pressure drop reaches 1.7 Pa for $h/H=0.35$, whereas the maximum ΔP's for $h/H=0.15$ and 0.25 are found to be only 0.3 and 0.7 Pa, respectively.

Optimization. The numerical and experimental results obtained so far are used to generate response surfaces for the heat

Downloaded From: http://electronicpackaging.asmedigitalcollection.asme.org/ on 08/21/2016 Terms of Use: http://www.asme.org/about-asme/terms-of-use



(*a*)



(*b*)

Fig. 14 Numerical and experimental heat transfer rates as a function of Re and h/H for $d=2w$ (*a*) first heat source and (*b*) second heat source

transfer rates from the heat sources and for the pressure drop as a function of the design variables Re, d, and h/H. Both second and third order response surfaces are generated, however, the coefficients of the third order terms are found to small compared to the first and second order terms. Thus, only second order response surfaces are presented. The variables are first normalized for more accurate coefficient calculation, and once the regression coefficients are calculated the variable are converted back to their actual values. The normalized variables are of the form:

$$\overline{\mathrm{Re}} = \frac{\mathrm{Re} - \mathrm{Re}_{\min}}{\mathrm{Re}_{\max} - \mathrm{Re}_{\min}} \quad \bar{d} = \frac{d/w - d/w_{\min}}{d/w_{\max} - d/w_{\min}} \quad \bar{h} = \frac{h/H - h/H_{\min}}{h/H_{\max} - h/H_{\min}} \tag{14}$$

The problem is a multi-objective design optimization problem, where the objectives are maximizing the total heat transfer rate, Q, minimizing the pressure drop, ΔP, and minimizing the material used for protrusions, S. Once the response surfaces are found for individual objectives, they can be combined to form a single objective function. Among several possible ways of combining the objectives into a single function, the weighted sums method, [27], is employed in the form of:

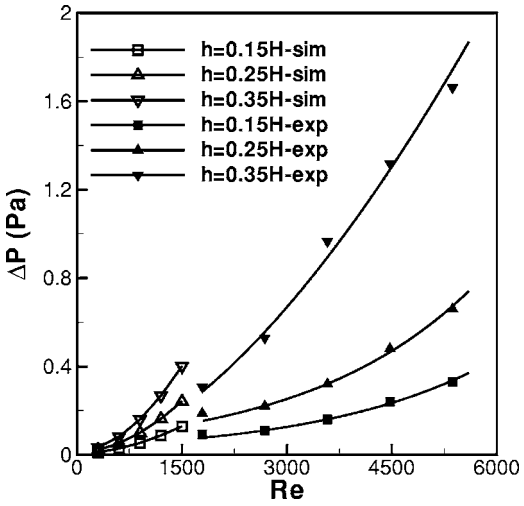
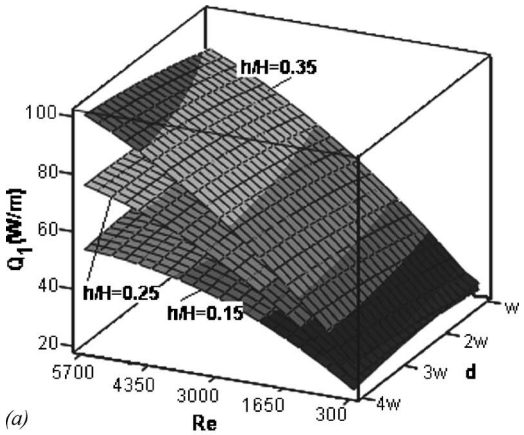


Fig. 15 Numerical and experimental pressure drop as a function of Re and h/H for $d=2w$

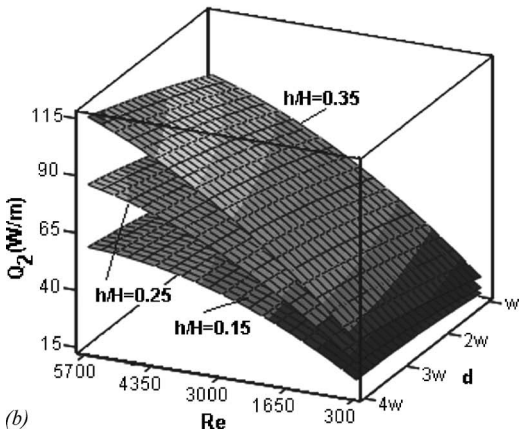
$$F = \sum W_i F_i(x_1, x_2, x_3) \tag{15}$$

where the $W_i (\in [0,1])$ is the weight of the ith objective function, and $\Sigma W_i = 1$.

The individual objective functions are shown first, in Figs. 16 and 17. The correlation coefficients R^2 and R^2_{adj} for the objective functions are tabulated in Table 2. The R^2 and R^2_{adj} values are observed to be very close indicating a successful response surface.



(*a*)



(*b*)

Fig. 16 Heat transfer rates response surfaces (*a*) first heat source and (*b*) second heat source

Downloaded From: http://electronicpackaging.asmedigitalcollection.asme.org/ on 08/21/2016 Terms of Use: http://www.asme.org/about-asme/terms-of-use

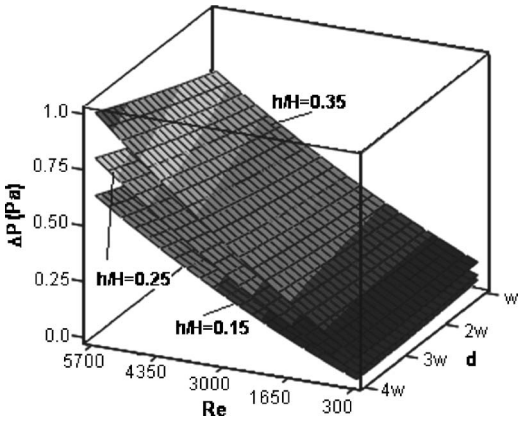


Fig. 17 Response surface of the pressure drop

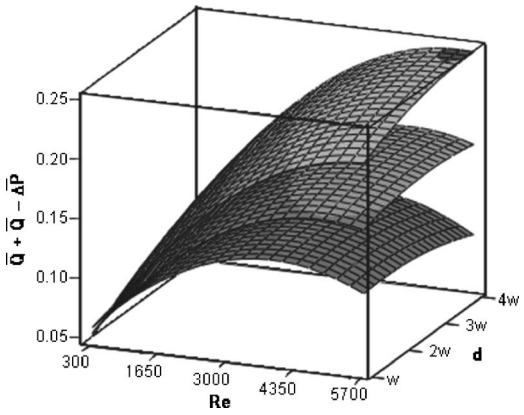


Fig. 18 Response surface of the objective function $F = W_1\overline{Q_1} + W_2\overline{Q_2} - W_3\Delta\bar{P}$, where $W_1 = W_2 = W_3$

All the R^2 and R^2_{adj} values are found to be greater than 0.85.

All the responses are observed to have similar trends, that is, the objective function value monotonically increases with all the design variables, Re, d and h/H. This leads to the conclusion that if the heat transfer rate is the sole objective the maximum values of Re, d, and h/H would be the optimal point. On the other hand, the single objective of minimizing the pressure drop results in the minimum values of the design variables. Therefore, a new objective function is to be defined which combines the heat transfer rate and the pressure drop. This is accomplished by adding objective functions in their normalized forms. The normalization is performed using the minimum and maximum values of the objective functions such that:

$$\overline{Q_i} = \frac{Q_i - Q_{i\min}}{Q_{i_{\max}} - Q_{i_{\min}}} \quad \text{and} \quad \overline{\Delta P} = \frac{\Delta P - \Delta P_{\min}}{\Delta P_{\max} - \Delta P_{\min}} \tag{16}$$

where i denotes the ith heat source.

The response surface of the new objective function, i.e., $F = W_1\overline{Q_1} + W_2\overline{Q_2} - W_3\Delta\bar{P}$, is depicted in Fig. 18. Since there are three design variables, the response is actually a volume. In order to effectively display the generated response, slices of surfaces at $h/H = 0.15$, 0.25, and 0.35 are shown on the graphs.

The global optimal points and the value of the objective function for various weights are tabulated in Table 3. It is observed that as the weight of the pressure drop is decreased to $W_1/2$ the optimal point is found at the maximum values of the design variables. This is because the maximum heat transfer rates are obtained at the same point, and making ΔP less important by setting its weight at a smaller value shifts the optimal point to the maximum values of the design variables. However, as the importance of ΔP increases, the optimal values of the design variables get smaller. When W_3 is set $2 \times W_1$ and $3 \times W_1$ the optimal value of Re drops to 2855 and 1450, respectively. The optimal heat source height is found to be either $h/H = 0.35$ or 0.15 depending on the relative importance of the individual objective functions. If maximizing the heat transfer rates is the primary design objective, the optimal h/H is found to be 0.35. If minimizing the pressure drop is more important than the heat transfer rate, then the desired value of h/H is 0.15.

The optimal values of Re and d for a given of h/H, when the performance of individual heat sources is of interest, are presented in Fig. 19. The results reveal that the optimal Re value does not change significantly with h/H. For the objective function of maximizing $\overline{Q_1} - \Delta\bar{P}$, Re^* falls in the range of 3000–3400, and for the objective function of $\overline{Q_2} - \Delta\bar{P}$, it varies between 1900 and 2200. The optimal separation distance, which maximizes $\overline{Q_1} - \Delta\bar{P}$, is found to be w, for h/H ratio of up to 0.2, and then displays an increase proportional to h/H. The separation distance desired to maximize $\overline{Q_2} - \Delta\bar{P}$ is observed to be greater than the former values, since the effect of the separation distance, on the heat transfer rates, is more profound on the second heat source than the first one.

The design of cooling systems for electronic equipment may also include minimization of the amount of material used as the heat sink in addition to maximization of the heat transfer rate and minimization of the pressure drop. The new problem can be formulated in terms of normalized objective functions in the following form:

$$F = W_1\overline{Q_1} + W_2\overline{Q_2} - W_3\Delta\bar{P} - W_4\bar{S} \tag{17}$$

where $\bar{S}$ is the amount of material used as the heat sink in normalized form. Because the present study deals with two-dimensional configuration, S can be written as material used per unit length or simply as the cross sectional area times the density of the material:

$$S = h \times w \times \rho_{\text{copper}} \tag{18}$$

and can be normalized by:

$$\bar{S} = \frac{S - S_{\min}}{S_{\max} - S_{\min}} \tag{19}$$

Assuming all the weights to be equal, i.e., $W_1 = W_2 = W_3 = W_4$, the response of the new objective function is calculated, as depicted in Fig. 20. The optimal values of the design variables, Re, d, and h/H, are tabulated for various weight combinations in Table 4.

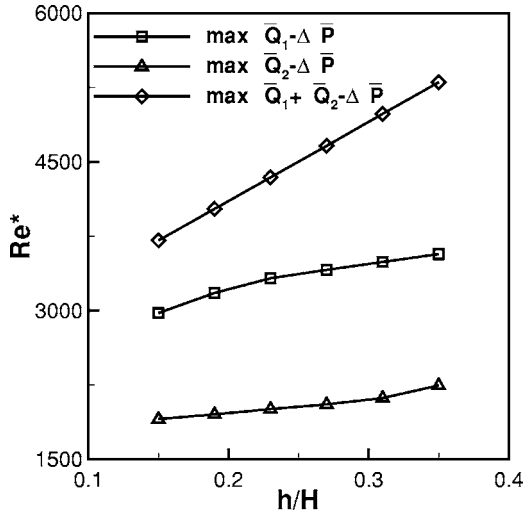
Table 2 Correlation coefficients of the response surfaces

	Q_1	Q_2	ΔP
R^2	0.90	0.93	0.87
R^2_{adj}	0.88	0.92	0.85

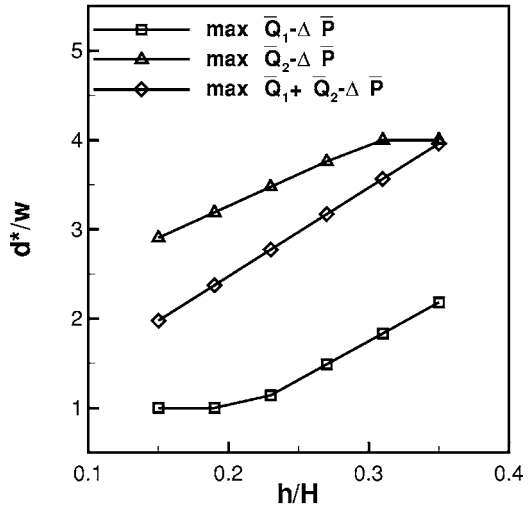
Table 3 Optimal points for different weights for the objective function $F = W_1\overline{Q_1} + W_2\overline{Q_2} - W_3\Delta\bar{P}$

	Re^*	d/w^*	h/H^*	Objective value
$W_1 = W_2 = W_3$	5300	3.96	0.35	0.334
$W_1 = W_2 = 2 \times W_3$	5600	4	0.35	0.600
$W_1 = W_2 = W_3/2$	2855	3.2	0.35	0.087
$W_1 = W_2 = W_3/3$	1450	2	0.15	0.026
$W_1 = W_2 = W_3/4$	300	3.2	0.18	0.019

Downloaded From: http://electronicpackaging.asmedigitalcollection.asme.org/ on 08/21/2016 Terms of Use: http://www.asme.org/about-asme/terms-of-use



(*a*)



(*b*)

Fig. 19 Optimal values of (*a*) Re and (*b*) *d*, with *h*/*H* for various objective functions

The results show that the optimal design variables vary substantially, and strongly depend on the formulation of the objective function and design priority.

Liquid Cooling Results. Forced convection liquid cooling experiments are performed for Re in the range of 2800–8500 and results are presented in Figs. 21 and 22. Figure 21 shows the Nu_{av} of heat sources as a function Re. It is observed that, for both the sources, the average heat transfer rate increases with Re and with the separation distance. For the first heat source the amount of enhancement in heat removal rate by increasing the separation distance is almost the same at all Re values. However, for the second heat source the rate of increase in heat transfer rate decreases with Re. For $d=2.5w$, Nu_{av} values of both heat sources are very close, whereas for $d=0.5w$, the second heat source has a higher Nu_{av}.

The results on the variation of the heat transfer coefficient with the heat input and with Re, when $d=0.5w$, as shown in Fig. 22, indicate that the heat input does not have any significant effect on the heat transfer coefficient. Re is the dominant factor, which affects the heat transfer coefficient. It is found that the heat transfer coefficient increases for both the heat sources with Re. Moreover, the second heat source heat transfer coefficient is found to be a few percent greater than that of the first heat source. There is almost no difference between the two at Re=2800 and the most significant difference is observed at Re=5800.

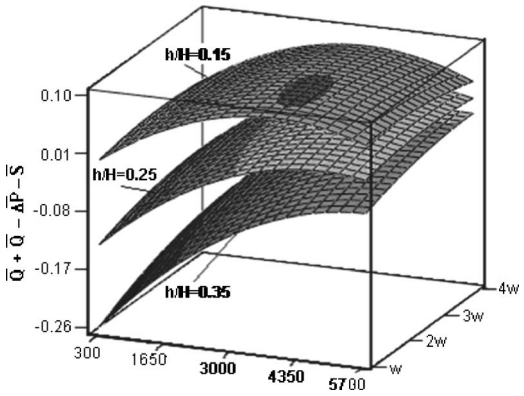


Fig. 20 Response surface of the objective function $F=W_1\overline{Q_1}+W_2\overline{Q_2}-W_3\Delta\bar{P}-W_4\bar{S}$ where $W_1=W_2=W_3=W_4$

The liquid cooling results presented here are for turbulent flow conditions. Similar to discussion made for air cooling, the switch between experiment and simulation can be carried out for liquid cooling as the flow changes from laminar to turbulent flow. Also, numerical modeling would be more efficient than experiment for simulating different channel dimensions and materials, whereas the experiment will be more efficient for changing the heat input and the flow rate.

A comparison of cooling capabilities of natural convection of air and de-ionized water is also performed, as shown in Fig. 23. Results display that the heat transfer coefficients for water are much greater than those for air, as expected, being around 19 times as high. The maximum heat transfer coefficient attained when $d=3.5w$ is found to be 18 W/m^2 K for air and 350 W/m^2 K for water. Overall, the heat transfer trends are similar to those for air. These results for liquid cooling are presented to compare the transport in different fluids, to show that the basic trends are similar, allowing the same concurrent experiment/numerical approach to be used, and to introduce the fluid as a possible design variable for system optimization.

Conclusions

The effects of Re, separation distance, and protrusion heights on the heat transfer rates from the heat sources and pressure drop along the channel are investigated. It is found that both the heat transfer rates and the pressure loss increase with all the three parameters. Among these design variables, the heat source height is found to have the most profound effect on ΔP, causing about 200% increase as h/H is changed from 0.25 to 0.35 at Re=5600. The same change in h/H is observed to result in as much as 100% increase in the heat transfer from the heat sources.

The optimization of the flow conditions, heat source height and separation distance of heat sources is performed for a multicriteria design optimization problem, in which the objectives are maximizing heat transfer rates, minimizing pressure drop, and minimizing heat sink material used. First, the critical operating condition at which transition from laminar to unsteady flow occurs is determined. This critical value is found to be Re=1500 and used as a criteria to switch from simulation to experiment. For the operating conditions of Re>1500, the numerical simulation starts losing accuracy, and the computational time increases dramatically. Thus, experimental approach is employed for inputs for design in turbulent flow regime. Then, the numerical and experimental results, obtained for different operating conditions and geometries, are combined to generate response surfaces of the objective functions. The optimal values of Re, heat source height,

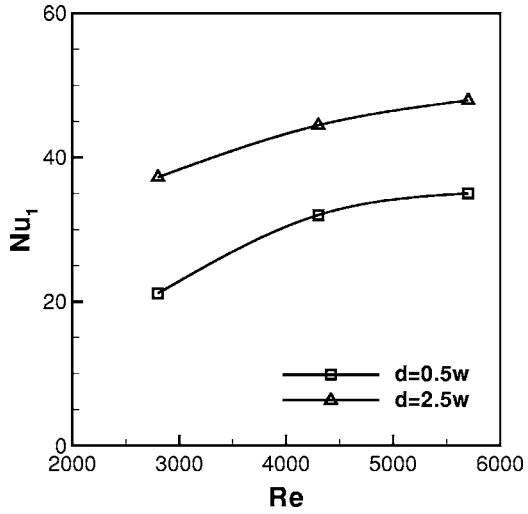
Downloaded From: http://electronicpackaging.asmedigitalcollection.asme.org/ on 08/21/2016 Terms of Use: http://www.asme.org/about-asme/terms-of-use

Table 4 Optimal points for different weights for the objective function $F = W_1\overline{Q_1} + W_2\overline{Q_2} - W_3\Delta\bar{P} - W_4\bar{S}$

	Re*	d/w^*	h/H^*	Objective value
$W_1=W_2=W_3=W_4$	3710	1.98	0.15	0.102
$W_1=W_2=W_3=2\times W_4$	5300	3.96	0.35	0.144
$W_1=W_2=W_3=3\times W_4$	5300	3.96	0.35	0.201
$W_1=W_2=W_4=2\times W_3$	4577	2.74	0.15	0.160
$W_1=W_2=W_4=3\times W_3$	5600	4	0.35	0.200
$W_1=W_2=W_4=W_3/2$	2530	1.57	0.15	0.045
$W_1=W_2=W_4=W_3/3$	1460	2	0.15	0.021
$W_1=W_2=W_3=W_4/2$	3705	2	0.15	0.081
$W_1=W_2=W_3=W_4/3$	3705	2	0.15	0.068

and separation distance are found for various objective functions. The optimal Re values for a given protrusion height are observed to be greater for the first heat source than the second source, whereas the optimal spacing which maximizes Q_2 is found to be greater than that of Q_1. The optimal values of the design variables, which maximize the combined objective function, i.e., $F = W_1\overline{Q_1} + W_2\overline{Q_2} - W_3\Delta\bar{P} - W_4\bar{S}$, are found as $\mathrm{Re}^* = 3710$, $d^*/w = 1.98$, and $h^*/H = 0.15$.

This study showed that the concurrent use of simulation and



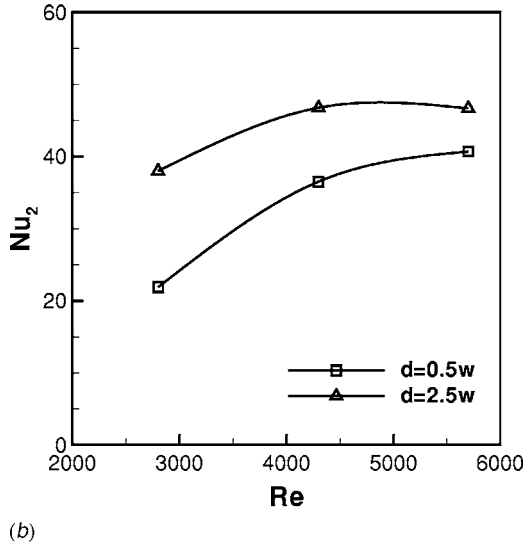
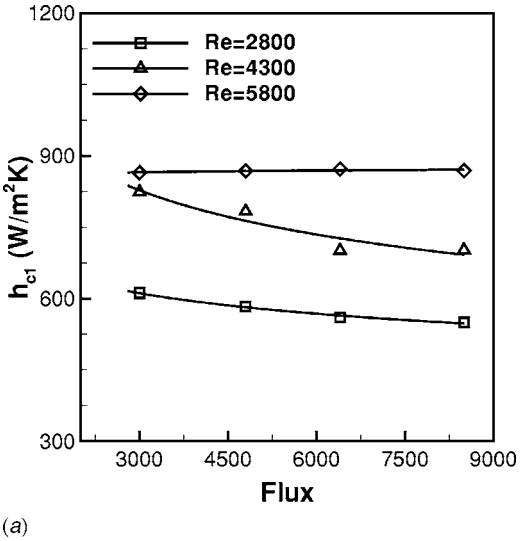


Fig. 21 Experimental results on Nu_{av} for water as a function of Re for (*a*) first heat source, (*b*) second heat source



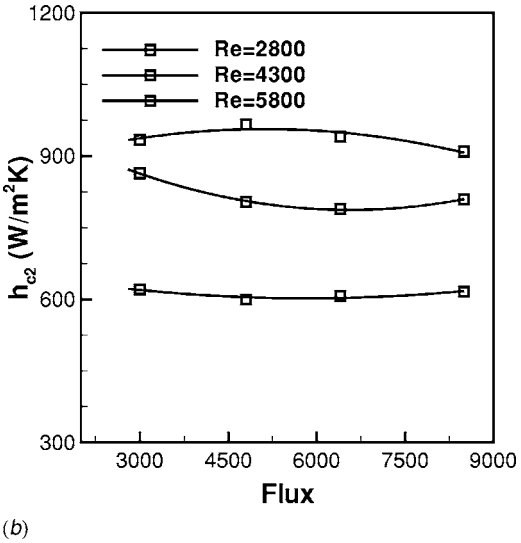
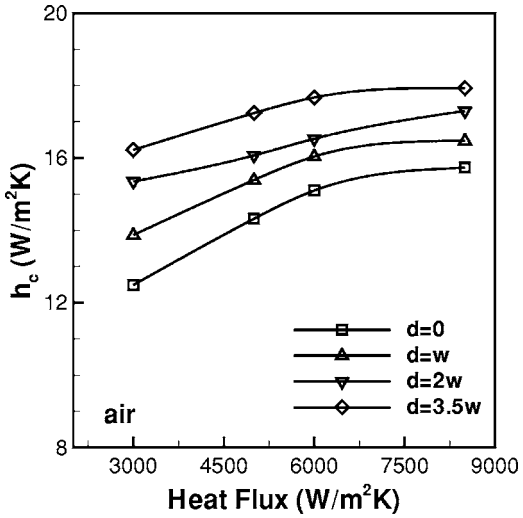
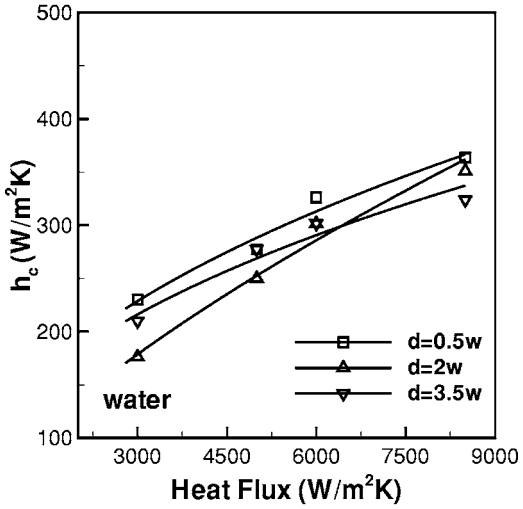


Fig. 22 Experimental heat transfer coefficient for water as a function of heat input and Re for (*a*) first heat source, (*b*) second heat source

Downloaded From: http://electronicpackaging.asmedigitalcollection.asme.org/ on 08/21/2016 Terms of Use: http://www.asme.org/about-asme/terms-of-use



(*a*)



(*b*)

Fig. 23 Comparison of experimental cooling capacities of natural convection in (*a*) air and (*b*) water

experiment improves the efficiency of design optimization by providing accurate and more reliable results as design inputs and by extending the search domain, compared to traditional design approaches. The performance of the methodology can further be improved by dynamically choosing the data points, and dynamically updating the response surfaces to minimize the number of data points required for design optimization.

Acknowledgment

The authors acknowledge the financial support provided by the National Science Foundation, under Grant No. CTS-0121058, for this work.

Nomenclature

B = bottom plate thickness
C_{hs} = surface length of the heat sources exposed to convection
d = separation distance
$\bar{d}$ = normalized separation distance $\in [0,1]$
e = uncertainty
F = objective function
g = gravitational acceleration
Gr = Grashof number, Eq. (7)
H = channel height
h = heat source height
h_{av} = average convective heat transfer coefficient
h_c = convective heat transfer coefficient
L = channel length
n = outward normal direction
Nu_{av} = average Nusselt number
Nu = local Nusselt number
P = dimensionless pressure
p = pressure
ΔP = pressure drop
$\Delta\bar{P}$ = normalized pressure drop $\in [0,1]$
ΔP_o = maximum allowable pressure drop
Pr = Prandtl number
$\underline{\mathrm{Re}}$ = Reynolds number based on channel height
$\overline{\mathrm{Re}}$ = normalized Reynolds number $\in [0,1]$
R^2 = coefficient of multiple determinations
R^2_{adj} = adjusted R^2 value
S = surface length of heat sources
$\bar{S}$ = normalized surface length of heat sources $\in [0,1]$
T = temperature
t = time
T_0 = ambient temperature
T_{wo} = maximum allowable component temperature
T_s = heat source temperature
V = velocity vector
W = width of the channel and weight coefficients of individual objective functions
w = heat source width
Q = heat input to the heat sources
$\bar{Q}$ = normalized heat transfer rate $\in [0,1]$
Q_t = total heat transfer rate from all heat sources

Greek Symbols

β = coefficient of thermal expansion, Eq. (7)
ν = kinematic viscosity
ρ = density of fluid
ρ_0 = fluid density at ambient temperature
τ = dimensionless time
θ = dimensionless temperature, Eq. (6).

References

[1] Incropera, F. P., 1988, "Convection Heat Transfer in Electronic Equipment Cooling," ASME J. Heat Transfer, **110**, pp. 1097–1111.
[2] Sathe, S., and Sammakia, B., 1998, "A Review of Recent Developments in Some Practical Aspects of Air-Cooled Electronic Packages," ASME J. Heat Transfer, **120**, pp. 830–839.
[3] Goldstein, R. J., Eckert, E. R. G., Ibele, W. E., Patankar, S. V., Simon, T. W., Kuehn, T. H., Strykowski, P. J., Tamma, K. K., Bar-Cohen, A., Heberlein, J. V. R., Davidson, J. H., Bischof, J., Kulakci, F. A., Kortshagen, U., and Garrick, S., 2002, "Heat Transfer – A Review of 2000 Literature," Int. J. Heat Mass Transfer, **45**, pp. 2853–2957.
[4] Kang, B. H., and Jaluria, Y., 1990, "Mixed Convection Transport From a Protruding Heat Source Module on a Vertical Surface," J. Thermophys. Heat Transfer, **4**(3), pp. 384–390.
[5] Tewari, S. S., and Jaluria, Y., 1990, "Mixed Convection Heat Transfer From Thermal Sources Mounted on Horizontal and Vertical Surfaces," ASME J. Heat Transfer, **112**, pp. 975–987.
[6] Papanicolaou, E., and Jaluria, Y., 1990, "Mixed Convection From an Isolated Heat Source in a Rectangular Enclosure," Numer. Heat Transfer, Part A, **18**, pp. 427–461.
[7] Nakayama, W., and Park, S. H., 1996, "Conjugate Heat Transfer From a Single Surface-Mounted Block to Forced Convective Air Flow in a Channel," ASME J. Heat Transfer, **118**, pp. 301–309.
[8] Kim, S. Y., Sung, H. J., and Hyun, J. M., 1992, "Mixed Convection From Multiple-Layered Boards With Cross-Streamwise Periodic Boundary Conditions," Int. J. Heat Mass Transfer, **35**(11), pp. 2941–2952.
[9] Rahman, M. M., and Raghavan, J., 1999, "Transient Response of Protruding Electronic Modules Exposed to Horizontal Cross Flow," Int. J. Heat Mass Transfer, **20**, pp. 48–59.
[10] Wang, Q., and Jaluria, Y., 2002, "Unsteady Mixed Convection in a Horizontal

Downloaded From: http://electronicpackaging.asmedigitalcollection.asme.org/ on 08/21/2016 Terms of Use: http://www.asme.org/about-asme/terms-of-use

Channel With Protruding Heating Blocks and a Rectangular Vortex Promoter," Phys. Fluids, **14**, pp. 2109–2112.
[11] Herman, C., Kang, E., Huang, H., and Puranik, B., 1995, "Experimental Visualization of Unsteady Temperature Fields in Electronic Cooling Applications," ASME Cooling and Thermal Design of Electronic Systems, EEP, 15, HTP 319.
[12] Kim, S. Y., Kang, B. H., and Jaluria, Y., 1998, "Thermal Interaction Between Isolated Heated Electronic Components in Pulsating Channel Flow," Numer. Heat Transfer, Part A, **34**, pp. 1–21.
[13] Ghaddar, N. K., Korczak, K. Z., and Mikic, B. B., 1986, "Numerical Investigation of Incompressible Flow in Grooved Channels. Part 1-Stability and Self-Sustained Oscillations," J. Fluid Mech., **163**, pp. 99–127.
[14] Nigen, S. J., and Amon, C. H., 1994, "Time-Dependent Conjugate Heat Transfer Characteristics of Self-Sustained Oscillatory Flows in a Grooved Channel," ASME J. Fluids Eng., **116**, pp. 499–507.
[15] Lin, W. L., and Lin, T. F., 1996, "Experimental Study of Unstable Mixed Convection of Air in a Bottom Heated Horizontal Rectangular Duct," Int. J. Heat Mass Transfer, **39**(8), pp. 1649–1663.
[16] Sathe, S. B., and Joshi, Y., 1992, "Natural Convection Liquid Cooling of a Substrate-Mounted Protrusion in a Square Enclosure: A Parametric Study," ASME J. Heat Transfer, **114**, pp. 401–409.
[17] Gupta, A., and Jaluria, Y., 1998, "Forced Convective Liquid Cooling of Arrays of Protruding Heated Elements Mounted in a Rectangular Duct," ASME J. Electron. Packag., **120**, pp. 243–252.
[18] Park, K. A., and Bergles, A. E., 1988, "Convective Heat Transfer in Electronic Equipment Cooling," ASME J. Heat Transfer, **110**, pp. 1097–1109.
[19] Joshi, Y., Kelleher, M. D., Powell, M., and Torres, E. I., 1991, "Natural Convection Heat Transfer From Array of Rectangular Protrusions in an Enclosure Filled With Dielectric Fluid," Heat Transfer Enhancement in Electronic Cooling, **183**, pp. 9–18.
[20] Incropera, F. P., Kerby, J. S., Moffatt, D. F., and Ramadhyani, S., 1986, "Convection Heat Transfer From Discrete Heat Sources in a Rectangular Channel," Int. J. Heat Mass Transfer, **20**, pp. 48–59.
[21] Jaluria, Y., 1998, *Design and Optimization of Thermal Systems*, McGraw-Hill, New York, pp. 32–148.
[22] Knight, D., Elliott, G., Jaluria, Y., Langrana, N., and Rasheed, K., 2002, "Automated Optimal Design Using Concurrent Integrated Experiment and Simulation," *AIAA Paper No. 2002-5636*, AIAA/ISSMO Symposium on Multidisciplinary Analysis and Optimization, Atlanta, Sept. 4–6.
[23] Zhao, H., Icoz, T., Jaluria, Y., and Knight, D., 2004, "Data Driven Design Optimization Methodology - Part I," AIAA Paper No. 2004-448, *42nd AIAA Aerospace Sciences Meeting and Exhibit*, Reno, NV, Jan. 5–8.
[24] Icoz, T., and Jaluria, Y., 2005, "Design of Cooling Systems for Electronic Equipment Using Both Experimental and Numerical Inputs," ASME J. Electron. Packag., **126**(4), pp. 465–471.
[25] Patankar, S. V., 1980, *Numerical Heat Transfer and Fluid Flow*, Hemisphere, New York, pp. 126–134.
[26] Papanicolaou, E., and Jaluria, Y., 1992, "Transition to a Periodic Regime in Mixed Convection in a Square Cavity," J. Fluid Mech., **239**, pp. 489–509.
[27] Deb, K., 2002, *Multi-Objective Optimization Using Evolutionary Algorithms*, Wiley, New York, pp. 49–55.

Downloaded From: http://electronicpackaging.asmedigitalcollection.asme.org/ on 08/21/2016 Terms of Use: http://www.asme.org/about-asme/terms-of-use